Journal of Thermal Analysis and Calorimetry (2020) 139:2321–2336
https://doi.org/10.1007/s10973-019-08617-7

Conjugate natural convection flow of Ag–MgO/water hybrid nanofluid in a square cavity

Mohammad Ghalambaz[1,2] · Ali Doostani[3] · Ehsan Izadpanahi[4] · Ali J. Chamkha[5]

Received: 10 May 2019 / Accepted: 19 July 2019 / Published online: 1 August 2019

Abstract

The conjugate natural convection of a new type of hybrid nanofluid (Ag–MgO/water hybrid nanofluid) inside a square cavity is addressed. A thick layer of conductive solid is considered over the hot wall. The governing partial differential equations (PDEs) representing the physical model of the natural convection of the hybrid nanofluid along with the boundary conditions are reported. The thermophysical properties of the nanofluid are directly calculated using experimental data. The governing PDEs are transformed into a dimensionless form and solved by the finite element method. The effect of the variation of key parameters, such as the volume fraction of nanoparticles, Rayleigh number, and the ratio between the thermal conductivity of the wall and the thermal conductivity of the hybrid nanofluid (R_k), is studied. Furthermore, the effects of the key parameters are investigated on the temperature distribution, local Nusselt number, and average Nusselt number. The results of this study show that the heat transfer rate increases by adding hybrid nanoparticles for a conduction-dominant regime (low Rayleigh number). The heat transfer rate is an increasing function of both the Rayleigh number and the thermal conductivity ratio (R_k). In the case of a convective-dominant flow (high Rayleigh number flow) and an excellent thermally conductive wall, the local Nusselt number at the surface of the conjugate wall decreases substantially by moving from the bottom of the cavity toward the top.

Keywords Conjugate natural convection · Hybrid nanofluid · Square cavity · Heat transfer enhancement

List of symbols

C	Specific heat (J kg^{-1} K^{-1})
C_p	Specific heat in constant pressure (J kg^{-1} K^{-1})
e^*	Wall thickness (m)
e	Non-dimensional wall thickness
g	Gravity (m s^{-2})
k	Thermal conductivity (W m^{-1} K^{-1})
P	Pressure (Pa)
T	Temperature (K)
H	Cavity size (length and height) (m)
Ra	Rayleigh number
Pr	Prandtl number
N	Number of nodes
Nu_{local}	Local Nusselt number
Nu_{avg}	Average Nusselt number
R_k	Thermal conductivity ratio
x, y	Cartesian coordinates
u	Fluid velocity component in the x-direction (m s^{-1})

✉ Mohammad Ghalambaz
mohammad.ghalambaz@tdtu.edu.vn

Ali Doostani
doostaniali@gmail.com

Ehsan Izadpanahi
eizad001@fiu.edu

Ali J. Chamkha
achamkha@pmu.edu.sa

[1] Department for Management of Science and Technology Development, Ton Duc Thang University, Ho Chi Minh City, Vietnam

[2] Faculty of Applied Sciences, Ton Duc Thang University, Ho Chi Minh City, Vietnam

[3] Department of Mechanical Engineering, Dezful Branch, Islamic Azad University, Dezful, Iran

[4] Department of Mechanical and Materials Engineering, Florida International University, Miami, FL 33174, USA

[5] Mechanical Engineering Department, Prince Mohammad Endowment for Nanoscience and Technology, Prince Mohammad Bin Fahd University, Al-Khobar 31952, Saudi Arabia

v Fluid velocity component in the y-direction (m s^{-1})
U Non-dimensional velocity component in the X-direction (m s^{-1})
V Non-dimensional velocity component in the Y-direction (m s^{-1})
X, Y Non-dimensional Cartesian coordinates

Greek symbols

α Thermal diffusivity (m^2 s^{-2})
ϕ Normalized volume fraction of nanoparticles
μ The fluid dynamic viscosity (kg m^{-1} s^{-1})
ξ Basis functions
ρ Density (kg m^{-3})
v Fluid kinematic-viscosity (m^2 s^{-1})
β Volumetric thermal expansion coefficient (1 K^{-1})
θ The non-dimensional temperature variable

Subscripts

bf Base fluid
c Cold wall
h Hot wall
hnf Hybrid nanofluid
nf Nanofluid
p Particles
s Solid (conjugate wall)

Introduction

During the past decade, nanofluids have been engineered as new working fluids with enhanced thermal conductivities. Since the time Choi and colleagues [1] synthesized the first type of nanofluid, various types of nanofluids have been developed using a range of types of nanoparticles and base fluids. For instance, TiO_2, SiO_2, Al_2O_3, CuO, Ag, Au, and MgO nanoparticles, as well as multi-wall carbon nanotubes (MWCNTs), nano-graphite sheets, nano-diamond particles, and clay nanoparticles have been utilized for the synthesis of nanofluids. Base fluids with relatively low thermal conductivities such as water, ethylene glycol, kerosene, and turbine oil have also been employed in the synthesis of nanofluids. In general, the result of suspending high-thermal conductive nanoparticles in a relatively low thermal conductive base fluid is an innovative nanofluid with enhanced thermophysical properties. Nanofluids show enhanced thermal conductivity, which makes them good candidates for heat transfer applications as working fluids in thermal systems. However, the theoretical and experimental results show that there are many cases, especially in natural-convection heat transfer applications, in which using nanofluids causes the heat transfer to deteriorate. This observed reduction in heat transfer can be attributed to the effect of the nano-sized additives on the dynamic viscosity of the nanofluid. Thus, using nanofluids for thermal enhancement requires careful attention and design. Mahian et al. [2, 3] reviewed the modeling approach and simulation of nanofluids.

There are well-established studies regarding the convective heat transfer of nanofluids, such as those used in [4–6]. There are also many practical cases involving the use of nanofluids for multi-purpose applications, which can be considered essential applications of nanoparticles. For example, the oil in an electrical power transformer acts as a dielectric material as well as a cooling medium. Due to natural convection, the oil moves between the electrical coils and the heat sinks mounted on the transformer's shell in most power transformers. Experimental studies of nanofluids reveal that dispersion of nano-diamond particles or silica nanoparticles in the transformer oil can enhance the dielectric properties of the oil. This increase in the dielectric properties of the utilized transformer oil is excellent and can justify using nanofluids in the transformers. However, the presence of a nanofluid may also enhance the heat transfer in the transformer, which can either be an excellent outcome or can jeopardize the thermal safety of the transformer due to the reduction in convective heat transfer in the power transformer.

Various aspects of convective heat transfer in cavities such as conjugate heat transfer [7], entropy generation [8], two phase nanofluid [9], magnetohydrodynamic effects [10], Marangoni effects [11], and heat transfer in porous media [12, 13] have been addressed in recent years.

A potentially interesting property of nanofluids has been noted by Kameya and Hanamura [14], who measured the radiation absorption characteristics of Ni nanoparticles in a nanofluid. By experimenting on visible to near-infrared wavelengths, Kameya and Hanamura [6] revealed that the absorption coefficient of the nanofluid suspension is much higher than that of the base liquid. Chen et al. [15] studied the radiation absorption characteristics of Ag, TiO_2, and ZnO nanoparticles suspended in water. In their investigation, silver nanoparticles are synthesized through a novel photochemical transformation. Their results demonstrate that Ag–water nanofluid has better radiation absorption than that of ZnO- and TiO_2-water nanofluids.

Moreover, the performance of low concentrations of a silver nanofluid is almost twice as that of the base fluid (water). It can be concluded that such nanofluids are suitable for use in solar ponds and in applications with radiation absorption. However, practical applications of these nanofluids require a careful heat transfer analysis. Padmavathy and Vijayaraghavan [16] addressed the anti-bacterial activity of ZnO nanoparticles with various particle sizes. They demonstrate that the anti-microbial bio-activity

of ZnO nanoparticles, and their bactericidal efficacy (i.e., their bacteria-killing property), increase with decreasing particle size. Bindhu and Umadevi [17] successfully utilized aqueous beetroot extract as a reducing agent for silver nanoparticle synthesis. They reported that prepared silver nanoparticles within the size of 15 nm are effective in inhibiting the growth of both gram-positive and gram-negative bacteria. Such anti-bacterial agents can be useful in the cooling of medical devices, sterilization systems, and food processing. However, the thermal behavior of such solutions is influenced by nano-additives. Hence, the thermal analysis of these newly engineered nanoparticles in base fluids requires careful analysis and design.

Important to note is that new types of nanofluids, called hybrid nanofluids, can be synthesized with enhanced properties. Hybrid nanofluids consist of different nanoparticles, either in a mixture or in a composite form dispersed in a base fluid. Hybrid nanofluids can lead to engineered fluids with adjusted thermophysical and chemical properties through a trade-off between the advantages and disadvantages of individual nanoparticles. In some cases, the nanoparticles can form a nano-composite structure in the base fluid which results in superior thermophysical properties much higher than those expected from each type of nanoparticle or their mixture. Such hybrid nanofluids can take advantage of the different nanoparticles in a mixture.

Considering the radiation absorption capabilities of Ag and TiO_2 nanoparticles in water, Xuan et al. [18] experimentally studied the optical properties of TiO_2 and Ag as well as hybrid TiO_2-Ag composite nanoparticles in a water-based nanofluid for solar energy absorption features. They showed that a TiO_2/Ag plasmonic nanofluid exhibits an absorption performance that was better than that of TiO_2, but similar to that of Ag. Although the thermal results for the Ag–water nanofluid and the TiO_2/Ag nanofluid were the same, the cost of the TiO_2/Ag-based nanofluid was much lower. Madhesh et al. [19] synthesized a Cu–TiO_2/water hybrid nanofluid, while Sundar et al. [20] synthesized an MWCNT–Fe_3O_4/water hybrid nanofluid. An excellent review of the practical applications and the recent development of hybrid nanofluids can be found in the work of Sarkar et al. [21].

Esfe et al. [22] synthesized samples of Ag–MgO/water hybrid nanofluids with up to a 2% volume concentration of nanoparticles. The hybrid nanofluid sample consists of 50% Ag and 50% MgO nanoparticles. In their study, the size of the silver nanoparticles was 25 nm, and the size of the magnesium oxide nanoparticles was 40 nm. The thermal conductivity and the dynamic viscosity of the synthesized hybrid nanofluid were measured for different nanoparticle volume fractions. Esfe et al. [22] demonstrated that both the thermal conductivity and the dynamic viscosity of the hybrid nanofluid are much higher than the individual nanofluids. Indeed, the nanoparticles in the base fluid form a nano-composite structure consisting of Ag and MgO nanoparticles. In another study, Esfe et al. [23] also synthesized samples of carbon nano-tube (CNT)–Al_2O_3/water hybrid nanofluids. They measured the thermal conductivity of the hybrid nanofluid for various temperatures and nanoparticle volume fractions. The outcomes show that the thermal conductivity of the nanofluid increases with the increase in temperature and nanoparticle volume fraction. Esfe et al. [24] successfully prepared samples of double-walled carbon nano-tubes, DWCNT (inner diameter of 3 nm) − ZnO (diameter of 10–30 nm)/water-ethylene glycol (60:40) hybrid nanofluids. They aimed to address the effect of the temperature and nanoparticle volume fraction upon thermal conductivity enhancement of the hybrid nanofluids. Their findings indicate that the thermal conductivity of the synthesized nanofluid is an increasing function of the temperature and nanoparticle volume fraction.

The literature review shows that a few studies have addressed hybrid nanofluid convection. For instance, Sundar et al. [20] studied the forced convection heat transfer and the pressure drop of MWCNT–Fe_3O_4/water hybrid nanofluids in the fully developed turbulent flow of a uniformly heated circular tube. In the case of a Reynolds number of 22,000, a 31.10% enhancement in the Nusselt number for a nanofluid containing 0.3% nanoparticles can be shown relative to base fluid data. However, the required pump power to maintain the same flow rate increases by 1.18 times.

Huang et al. [25] prepared samples of MWCNT/water and Al_2O_3/water nanofluids to form a hybrid nanofluid with a volume ratio of 1:2.5 (MWCNT:Al_2O_3). Specifically, a small portion of MWCNT is added to Al_2O_3 nanofluid to enhance the thermal conductivity of the Al_2O_3–water nanofluid further. The heat transfer enhancement of the MWCNT–Al_2O_3/water hybrid nanofluid, as well as that of Al_2O_3/water nanofluid in a chevron corrugated-plate heat exchanger, is then tested. The results reveal that the hybrid nanofluid mixture generates a smaller pressure drop compared to that of the Al_2O_3/water nanofluid. However, the pressure drop of the hybrid nanofluid is marginally higher than that of the base fluid (water). The hybrid nanofluid mixture also demonstrates the highest heat transfer coefficient for given pumping power.

Madhesh et al. [19] tested the thermal performance of Cu–TiO_2/water hybrid nanofluid in a tube-type counter flow heat exchanger. The results indicate a 68% increase in the overall heat transfer coefficient when using up to a 1.0% volume concentration of hybrid nanoparticles. However, up to 2.0% increase in the volume concentration of nanoparticles results in a marginal reduction in

convective heat transfer potential. A pressure drop, obtained by using a 2.0% volume concentration of the hybrid nanofluid, is reported to be 14.9%, which demonstrates a penalty in the pumping capacity. The forced convective heat transfer of hybrid nanofluids has also been studied in microchannels [26].

As another aspect of heat transfer of hybrid nanofluids in enclosures, Ghalambaz et al. [27] and Chamkha et al. [28] studied the convective heat transfer of hybrid nano-enhanced phase-change materials in enclosures. Mehryan et al. [29] addressed the heat transfer of hybrid nanofluids in an enclosure filled with a porous medium.

The study of conjugate heat transfer is necessary because it refers to the realistic modeling of heat transfer in many engineering applications involving heat transfer not only within, but also between, solid and fluid regions. There are many examples, such as heat transfer in the shell of a container (solid) filled with a liquid (fluid), heat transfer between a heat sink (solid) and its surrounding fluid (fluid), and heat transfer between the thick wall of a tube (solid) and the liquid inside the tube (fluid). These are only a few of the more straightforward applications of conjugate heat transfer.

Due to the importance and number of applications of conjugate heat transfer in the industrial sector, its properties have been investigated in recent years. For instance, Ben-Nakhi and Chamkha [30, 31] studied conjugate natural convective heat transfer in a cavity containing a solid fin. Shenoy et al. [32], who have examined the effect of the shape of either a hot or a cold surface, asserted that the shape of the surface could be an essential parameter for the rate of natural-convection heat transfer in an enclosure. Interestingly, the relevance of the properties of the medium has been noted by many other researchers. For instance, Sheremet et al. [33] explored the conjugate transient natural convection of nanofluids in an enclosure. Sheremet and Miroshnichenko [34] analyzed the effect of thick solid walls on the natural convection heat transfer in a cavity. Chamkha and Ismael [24, 25] investigated the conjugate heat transfer of pure fluids [35] as well as single nanofluids [36] in a cavity filled with a nanofluid and heated by a thick wall. Kuznetsov and Sheremet [37] studied the conjugate natural convection heat transfer of simple nanofluids in a cavity by considering the effect of the gradient of nanoparticles. Sheremet et al. [38] investigated the unsteady natural convection of nanofluids in a porous cavity. Sheremet and Pop [39] extended the study of Kuznetsov and Sheremet [37] on steady-state conjugate heat transfer in a porous medium by taking into account the non-uniform distribution of nanoparticles.

Some of the engineering applications of natural convective heat transfer in a cavity include heat storage systems in solar collectors enhanced with fins, heat removal in heat exchangers, and active nuclear waste disposal systems. Nanofluids are useful not only for heat transfer but also for other medical and electrical applications. Nanoparticles suspended in a fluid (nanofluids) can also be utilized for other purposes, such as nanoparticles serving as radiation-absorbent media, anti-microbial means. In such applications, the improvement of heat transfer, resulting from the use of nanoparticles in the base fluid, may be either an advantageous by-product or a disadvantage. Nevertheless, it is important to note that the use of hybrid nanoparticles as nano-additives can be multi-purpose. One type of nanoparticle may act as an anti-bacterial agent or absorbent, while the other nanoparticle may enhance heat transfer.

The present study aims to theoretically address the effects of using a hybrid nanofluid on the natural convection heat transfer in a cavity heated by a thick wall. Four key issues associated with the heat transfer aspects of hybrid nanofluids (here, Ag–MgO/water) have been addressed for the first time. Here, Ag–MgO/water nanofluid is adopted as an example of a synthesized hybrid nanofluid because synthesized samples of this type of hybrid nanofluid have been reported in the literature, so its thermophysical data are available. Moreover, silver nanoparticles are known to be anti-bacterial agents.

1. What happens to natural-convection heat transfer in the presence of hybrid nanofluids? Does the heat transfer enhance due to the improvement of thermal conductivity or deteriorate due to the augmentation of viscosity?
2. Is there any thermal advantage to utilizing water-based Ag–MgO hybrid nanofluid compared to a regular water-based nanofluid?
3. How does the cavity's wall thickness or material (thermal conductivity) affect the natural convection thermal behavior of hybrid nanofluids?
4. Does increasing the volume fraction of Ag–MgO nanoparticles in the base fluid always enhance heat transfer?

In order to answer the above fundamental key questions, we proceed to the next section to introduce a physical model for the flow and heat transfer of a hybrid nanofluid in a cavity.

Physical and mathematical models

The physical model

Figure 1 shows the schematic view of the physical model of the problem and its coordinate system. Consider a square cavity with the size of *H,* in which one of the walls has a

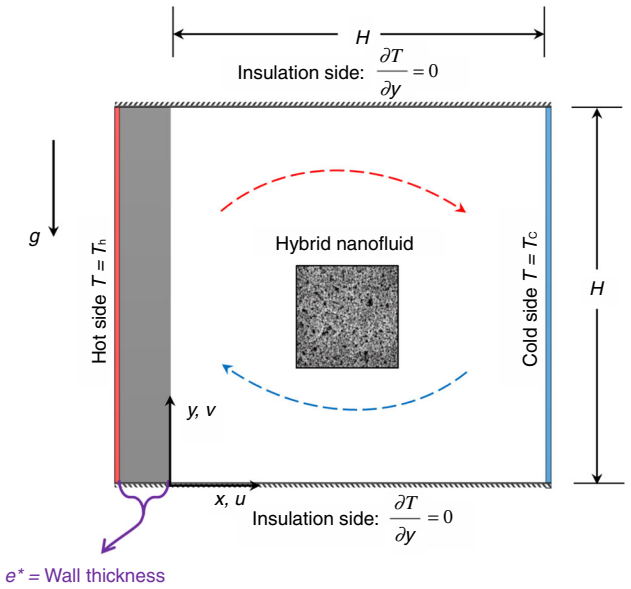

Fig. 1 Schematic view of the physical model in which the boundary condition of the left vertical wall is isothermal (B.C.: $T = T_H$)

Table 1 Thermophysical properties of the components of Ag (20 nm)–MgO (40 nm)/water hybrid nanofluid [40, 41]

Physical properties	Water	Ag	MgO
c_p/J kg^{-1} K^{-1}	4179	235	879
k/W m^{-1} K^{-1}	0.613	429	30
α/m^2 s^{-1}	1.47×10^{-7}	174×10^{-3}	95.3×10^{-7}
β/K^{-1}	21×10^{-5}	5.4×10^{-5}	33.6×10^{-6}
ρ/kg m^{-3}	997.1	10,500	3580
μ/kg m^{-1} s^{-1}	8.9×10^{-4}	–	–

thickness equal to e. The cavity is filled with a mixture of water and Ag–MgO hybrid nanoparticles. The thermophysical properties of water, Ag, and MgO are represented in Table 1. The bottom and top walls are assumed well-insulated. The right and the left vertical walls are kept at the isothermal temperatures of T_c and T_h, respectively.

Governing equations

Continuity

$$\nabla \cdot u = 0 \tag{1}$$

Momentum

$$(u \cdot \nabla)u = -\frac{1}{\rho_{hnf}}\nabla P + \frac{\mu_{hnf}}{\rho_{hnf}}\nabla^2 u + \beta_{hnf} g(T - T_f) \tag{2}$$

Energy

$$(u) \cdot \nabla T = \alpha_{hnf}\nabla^2 T \tag{3}$$

Equations (1)–(3) in the expanded form can be written as follows:

Continuity

$$\frac{\partial u}{\partial x} + \frac{\partial v}{\partial y} = 0 \tag{4}$$

Momentum in x-direction

$$\rho_{hnf}\left(u\frac{\partial u}{\partial x} + v\frac{\partial u}{\partial y}\right) = -\frac{\partial P}{\partial x} + \mu_{hnf}\left(\frac{\partial^2 u}{\partial x^2} + \frac{\partial^2 u}{\partial y^2}\right) \tag{5}$$

Momentum in y-direction

$$\rho_{hnf}\left(u\frac{\partial v}{\partial x} + v\frac{\partial v}{\partial y}\right) = -\frac{\partial P}{\partial y} + \mu_{hnf}\left(\frac{\partial^2 v}{\partial x^2} + \frac{\partial^2 v}{\partial y^2}\right) + \rho_{hnf} g\beta(T - T_f) \tag{6}$$

Energy

$$\left(u\frac{\partial T}{\partial x} + v\frac{\partial T}{\partial y}\right) = -\frac{k_{hnf}}{(\rho C_P)_{hnf}}\left(\frac{\partial^2 T}{\partial x^2} + \frac{\partial^2 T}{\partial y^2}\right) \tag{7}$$

Besides, the heat conduction equation for the temperature distribution in the left wall is introduced as:

$$k_s\left(\frac{\partial^2 T}{\partial x^2} + \frac{\partial^2 T}{\partial y^2}\right) = 0 \tag{8}$$

The boundary conditions are illustrated in the schematic figure, Fig. 1. Following Fig. 1, the boundary conditions can be introduced as follows:

$$\text{At the cooled wall } x = H,\ u = 0,\ v = 0,\ T = T_c \tag{9a}$$

$$\text{At the hot wall } x = -e^*,\ u = 0,\ v = 0,\ T = T_h \tag{9b}$$

$$\text{At the bottom wall } y = 0,\ u = 0,\ v = 0,\ \frac{\partial T}{\partial y} = 0 \tag{9c}$$

$$\text{At the top wall } y = H,\ u = 0,\ v = 0,\ \frac{\partial T}{\partial y} = 0 \tag{9d}$$

Here, e^* is the wall thickness, and H is the cavity size (height and width of the cavity). The boundary conditions on the interface of the heating wall in dimensional form are introduced as [42]:

$$k_{hnf}\left(\frac{\partial T}{\partial x}\right)_{hnf} = k_s\left(\frac{\partial T}{\partial x}\right)_s \text{ and } T_{hnf} = T_s \tag{10}$$

where $R_k = k_{hnf}/k_s$. To transform the governing equations, Eqs. (4)–(8), along with their boundary condition, Eq. (9), the following non-dimensional variables are utilized:

$$X = \frac{x}{H},\quad Y = \frac{y}{H},\quad U = \frac{uH}{\alpha_{bf}},\quad V = \frac{vH}{\alpha_{bf}},\quad \theta = \frac{T - T_f}{T_h - T_f},\quad \theta_s = \frac{T_s - T_f}{T_h - T_f},\quad P = \frac{PH^2}{\rho_{bf}\alpha_{bf}^2} \tag{11}$$

The Rayleigh number (Ra) and Prandtl number (Pr) are also introduced in the usual way as:

$$Ra = \frac{g\beta_{\mathrm{bf}}(T_{\mathrm{h}} - T_{\mathrm{f}})L^3}{\alpha_{\mathrm{bf}}\nu_{\mathrm{bf}}}, \quad Pr = \frac{\nu_{\mathrm{bf}}}{\alpha_{\mathrm{bf}}} \tag{12}$$

Additionally, the body force term can be written in Cartesian coordinates as follows:

$$\vec{F} = \rho_{\mathrm{hnf}}\beta\vec{g}(T - T_{\mathrm{f}}) \tag{13}$$

Invoking the non-dimensional parameters of Eq. (11), the governing equations, Eqs. (4)–(7), are transformed into a non-dimensional form as follows:

Continuity:

$$\frac{\partial U}{\partial X} + \frac{\partial V}{\partial Y} = 0 \tag{14}$$

Momentum in X-direction:

$$\left(\frac{\rho_{\mathrm{hnf}}}{\rho_{\mathrm{bf}}}\right)\left(U\frac{\partial U}{\partial X} + V\frac{\partial U}{\partial Y}\right) = -\frac{\partial P}{\partial X} + \frac{\mu_{\mathrm{hnf}}}{\mu_{\mathrm{bf}}}Pr\left(\frac{\partial^2 U}{\partial X^2} + \frac{\partial^2 U}{\partial Y^2}\right) \tag{15}$$

Momentum in Y-direction:

$$\left(\frac{\rho_{\mathrm{hnf}}}{\rho_{\mathrm{bf}}}\right)\left(U\frac{\partial V}{\partial X} + V\frac{\partial V}{\partial Y}\right) = -\frac{\partial P}{\partial Y} + \frac{\mu_{\mathrm{hnf}}}{\mu_{\mathrm{bf}}}Pr\left(\frac{\partial^2 V}{\partial X^2} + \frac{\partial^2 V}{\partial Y^2}\right) + PrRa\theta\frac{(\rho\beta)_{\mathrm{hnf}}}{(\rho\beta)_{\mathrm{bf}}} \tag{16}$$

Energy:

$$\left(\frac{(\rho c_p)_{\mathrm{hnf}}}{(\rho c_p)_{\mathrm{bf}}}\right)\left(U\frac{\partial \theta}{\partial X} + V\frac{\partial \theta}{\partial Y}\right) = \frac{k_{\mathrm{hnf}}}{k_{\mathrm{bf}}}\left(\frac{\partial^2 \theta}{\partial X^2} + \frac{\partial^2 \theta}{\partial Y^2}\right) \tag{17}$$

$$\frac{k_{\mathrm{s}}}{k_{\mathrm{bf}}}\left(\frac{\partial^2 \theta_{\mathrm{s}}}{\partial x^2} + \frac{\partial^2 \theta_{\mathrm{s}}}{\partial y^2}\right) = 0 \tag{18}$$

By using the dimensionless parameters in Eq. (11), the non-dimensional boundary conditions can be presented as:

$$\text{Cooled wall } X = 1: \quad U = 0,\ V = 0,\ \theta = 0 \tag{19a}$$

$$\text{Hot wall } X = -e: \quad U = 0,\ V = 0,\ \theta = 1 \tag{19b}$$

$$\text{Bottom wall } Y = 0: \quad U = 0,\ V = 0,\ \frac{\partial \theta}{\partial Y} = 0 \tag{19c}$$

$$\text{Top wall } Y = 1: \quad U = 0,\ V = 0,\ \frac{\partial \theta}{\partial Y} = 0 \tag{19d}$$

where $e = e^*/H$, which is the non-dimensional solid wall thickness. In the present study, e is assumed as $e = 0.2$. According to the non-dimensional variables, Eq. (10) can be rewritten in the form:

$$R_{\mathrm{k}}\left(\frac{\partial \theta}{\partial x}\right)_{\mathrm{hnf}} = \left(\frac{\partial \theta}{\partial x}\right)_{\mathrm{s}} \tag{20}$$

The heat transfer rate is represented by the Nusselt number, which can be defined by the following relationship:

$$Nu_{\mathrm{local}} = -\frac{k_{\mathrm{hnf}}}{k_{\mathrm{bf}}}\frac{\partial T}{\partial x}\bigg|x = 0 \tag{21}$$

The average Nusselt number Nu_{avg} is obtained by integrating the local Nusselt number Nu_{local}:

$$Nu_{\mathrm{avg}} = \int_0^1 Nu_{\mathrm{local}}\mathrm{d}y$$

In this equation, the effective density (ρ_{hnf}) and the thermal expansion coefficient ($\rho\beta)_{\mathrm{hnf}}$ for hybrid nanofluids can be defined as follows [43]:

$$\rho_{\mathrm{hnf}} = \rho_{\mathrm{bf}}(1 - \varphi_{\mathrm{hnf}}) + \rho_{\mathrm{Ag}}\varphi_{\mathrm{Ag}} + \rho_{\mathrm{MgO}}\varphi_{\mathrm{MgO}} \tag{22}$$

$$(\rho\beta)_{\mathrm{hnf}} = (\rho\beta)_{\mathrm{bf}}(1 - \varphi_{\mathrm{hnf}}) + (\rho\beta)_{\mathrm{Ag}}\varphi_{\mathrm{Ag}} + (\rho\beta)_{\mathrm{MgO}}\varphi_{\mathrm{MgO}} \tag{23}$$

where

$$\varphi_{\mathrm{hnf}} = \varphi_{\mathrm{Ag}} + \varphi_{\mathrm{MgO}} \tag{24}$$

In all the relations mentioned above, φ represents the volume fraction of nanoparticles. In Eq. (17), $\alpha_{\mathrm{hnf}} = k_{\mathrm{hnf}}/(\rho c_{\mathrm{p}})_{\mathrm{hnf}}$ denotes the thermal diffusivity of the hybrid nanofluid. Furtheremore, the thermal conductivity of the hybrid nanofluid is evaluated through curve fitting of the experimental data of Esfe et al. [22]:

$$\frac{k_{\mathrm{hnf}}}{k_{\mathrm{bf}}} = \frac{0.1747 \times 10^5 + \varphi_{\mathrm{hnf}}}{0.1747 \times 10^5 - 0.1498 \times 10^6\varphi_{\mathrm{hnf}} + 0.1117 \times 10^7\varphi_{\mathrm{hnf}}^2 + 0.1997 \times 10^8\varphi_{\mathrm{hnf}}^3} \quad 0 \le \varphi_{\mathrm{hnf}} \le 0.03 \tag{25}$$

Likewise, the experimental results of Esfe et al. [22] were extracted for different hybrid nanoparticle volume fractions to calculate the hybrid nanofluid's dynamic viscosity through curve fitting of the experimental data to yield the following values:

$$\frac{\mu_{\mathrm{hnf}}}{\mu_{\mathrm{bf}}} = \left(1 + 32.795\varphi_{\mathrm{hnf}} - 7214\varphi_{\mathrm{hnf}}^2 + 714600\varphi_{\mathrm{hnf}}^{3)} - 0.1941 \times 10^8 \varphi_{\mathrm{hnf}}^4\right) \quad 0 \le \varphi_{\mathrm{hnf}} \le 0.02 \tag{26}$$

Based on the data of the experimental study of Esfe et al. [22], the volume fractions of hybrid nanoparticles (50% Ag and 50% MgO by volume) in the present study are assumed to be between 0 and 2%. In the study of Esfe et al. [22], the Ag nanoparticles had a diameter of 25 nm, and the diameters of the MgO nanoparticles were equal to 40 nm. Similar values are assumed here.

Numerical solution

The finite element method [44] is employed to solve the system of partial differential equations (PDEs) of Eqs. (14)–(18) along with the corresponding boundary conditions of Eqs. (19) and (20). Based on the finite element method, the weak form of the governing equations is obtained and integrated numerically. To ensure the satisfaction of mass conservation, the continuity equation, Eq. (14), is invoked as a constraint to control the pressure distribution in the domain of the solution. Thus, as a penalty parameter, the following constraint equation is introduced and substituted in the momentum equations as described by [44]. In it, the pressure is introduced as:

$$P = \chi\left(\frac{\partial U}{\partial X} + \frac{\partial V}{\partial Y}\right) \tag{27}$$

where χ is a large number ($\chi = 10^7$ [44]) and denotes the penalty number. Using Eq. (27), the momentum equations, Eqs. (15) and (16), are obtained as:

$$\left(\frac{\rho_{\mathrm{hnf}}}{\rho_{\mathrm{bf}}}\right)\left(U\frac{\partial U}{\partial X} + V\frac{\partial U}{\partial Y}\right) = -\frac{\partial}{\partial X}\left(\chi\left(\frac{\partial U}{\partial X} + \frac{\partial V}{\partial Y}\right)\right) + \frac{\mu_{\mathrm{hnf}}}{\mu_{\mathrm{bf}}} Pr\left(\frac{\partial^2 U}{\partial X^2} + \frac{\partial^2 V}{\partial Y^2}\right) \tag{28}$$

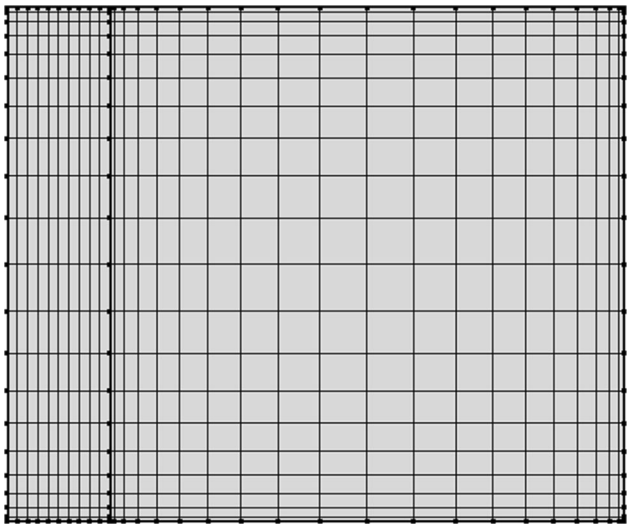

Fig. 2 A sample of the non-uniform structured mesh with the coarse size of 20 × 20 and an element ratio of 10

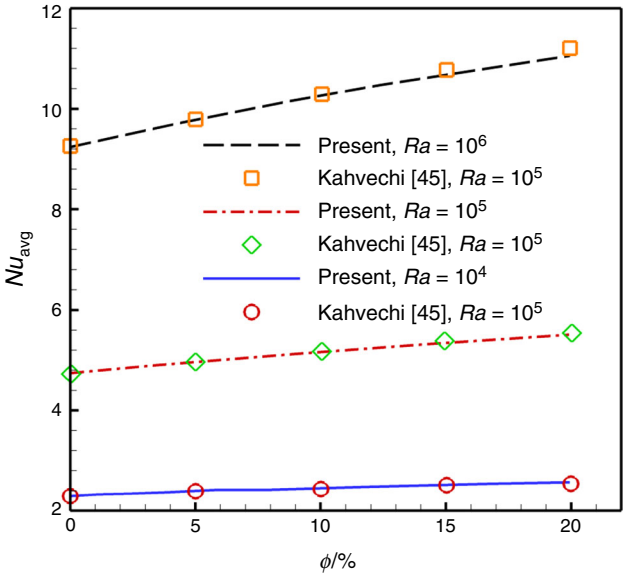

Fig. 3 A comparison between the results of the present study and Kahveci [45] for Nu_{avg} as a function of the volume fraction of nanoparticles when Ra = 10^4, 10^5 and 10^6

Table 2 Effects of different grid sizes versus the volume fractions of Ag–MgO hybrid nanoparticle on the average Nusselt number (Nu_{avg}), when Pr = 6.2 and R_{k} = 10 and the nanoparticle compositions are 50% Ag (25 nm) and 50% MgO (40 nm)

Rayleigh number (Ra)	Hybrid nanoparticles concentration/ϕ%	Grid size				
		50 × 50	70 × 70	100 × 100	120 × 120	140 × 140
10^4	0	2.1536	2.1530	2.1527	2.1527	2.1526
10^4	1	2.1490	2.1485	2.1483	2.1482	2.1482

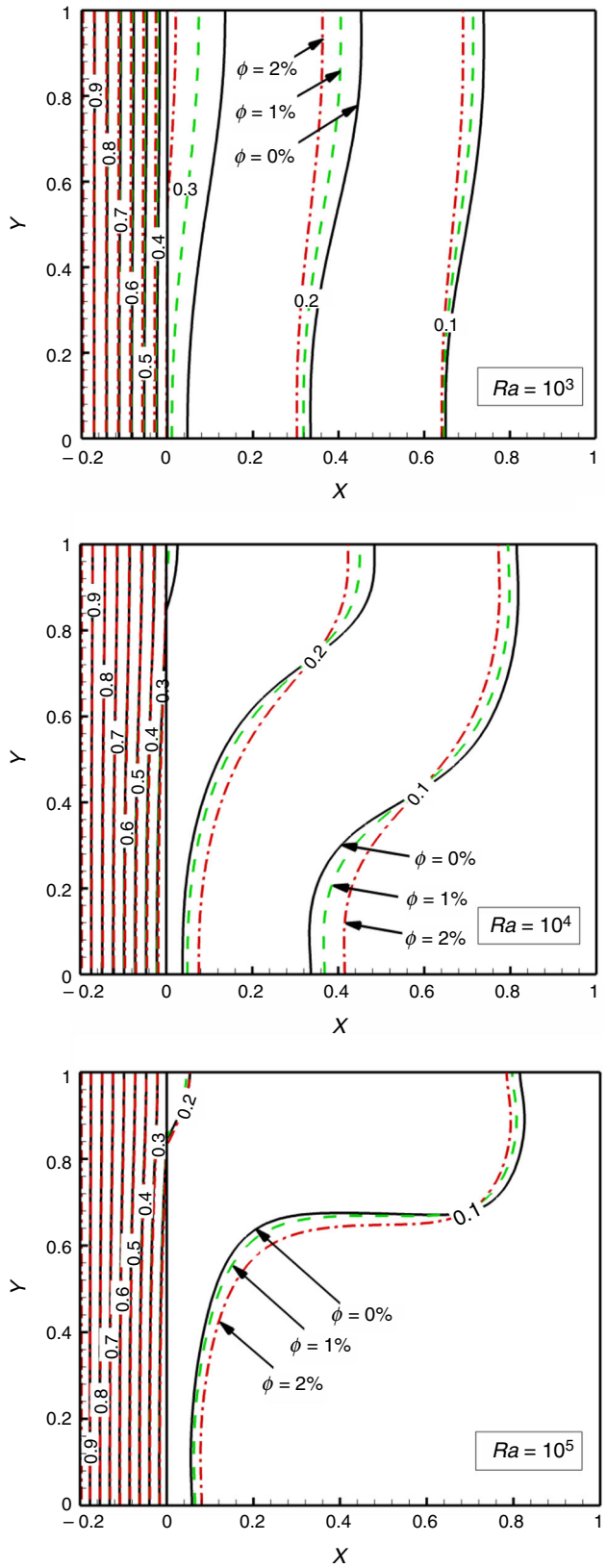

Fig. 4 The isothermal contours of hybrid nanofluid Ag–MgO/water for different values of the hybrid nanoparticle volume fraction at $Ra = 10^3$–10^5 for $R_k = 0.1$

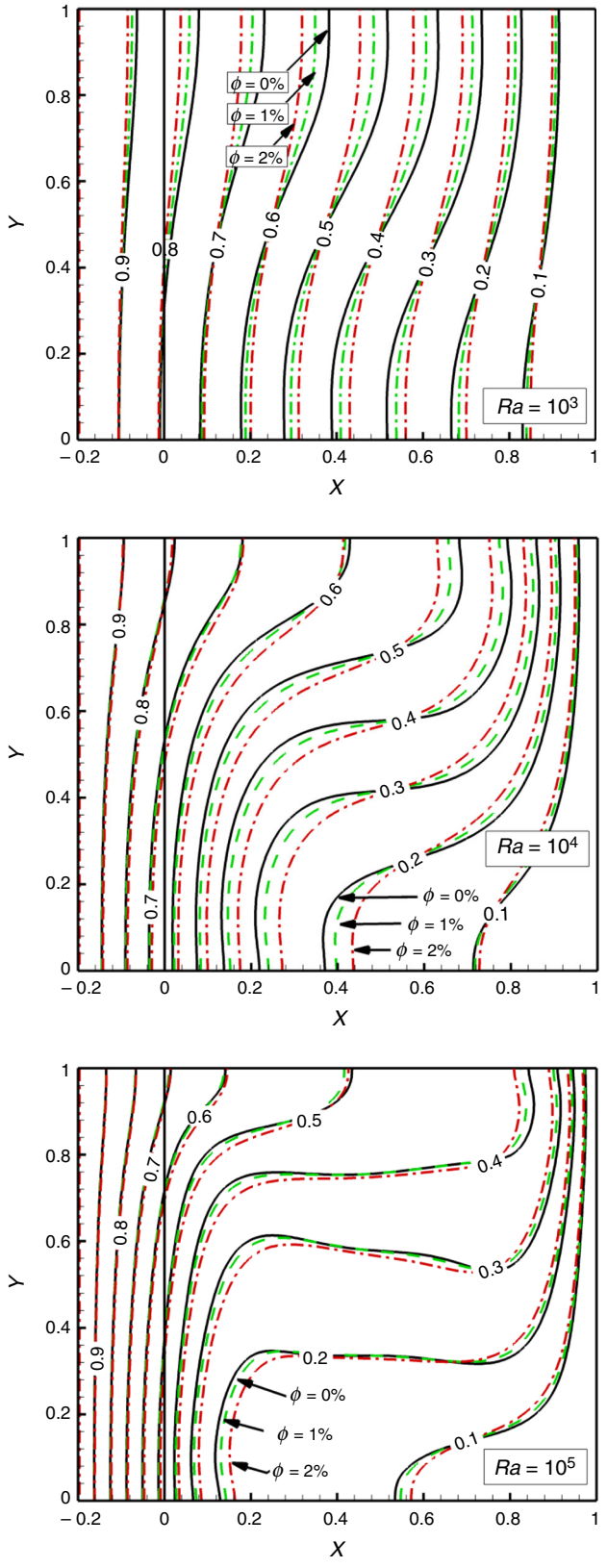

Fig. 5 The isothermal contours of hybrid nanofluid Ag–MgO/water for different values of the hybrid nanoparticle volume fraction at $Ra = 10^3$, 10^4, and 10^5 for $R_k = 1$

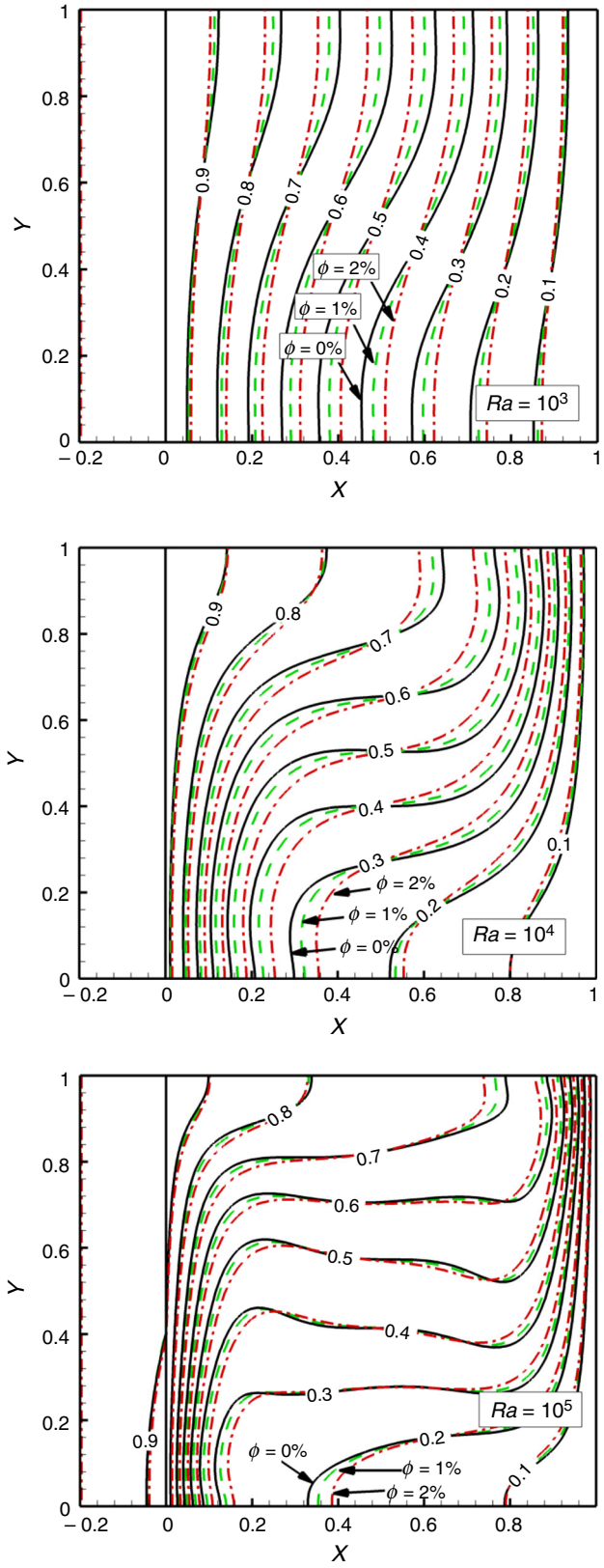

Fig. 6 The isothermal contours of hybrid nanofluid Ag–MgO/water for the different values of the hybrid nanoparticle volume fraction at $Ra = 10^3$, 10^4, and 10^5 for $R_k = 10$

$$\left(\frac{\rho_{hnf}}{\rho_{bf}}\right)\left(U\frac{\partial V}{\partial X}+V\frac{\partial V}{\partial Y}\right)=-\frac{\partial}{\partial Y}\left(\chi\left(\frac{\partial U}{\partial X}+\frac{\partial V}{\partial Y}\right)\right)+\frac{\mu_{hnf}}{\mu_{bf}}Pr\left(\frac{\partial^2 U}{\partial X^2}+\frac{\partial^2 V}{\partial Y^2}\right)+PrRa\theta\frac{(\rho\beta)_{hnf}}{(\rho\beta)_{bf}} \tag{29}$$

Now, by invoking a basis set $\{\xi_k\}_{k=1}^N$, the non-dimensional velocities of U and V along with the dimensionless temperatures of θ and θ_s are expanded as:

$$U\approx\sum_{k=1}^{N}U_k\xi(X,Y),V\approx\sum_{k=1}^{N}V_k\xi(X,Y),\theta\approx\sum_{k=1}^{N}\theta_k\xi(X,Y)\quad \text{at } 0<X<1 \text{ and } 0<Y<1 \tag{30}$$

and

$$\theta_s\approx\sum_{k=1}^{N}\theta s_k\xi(X,Y)\quad \text{at } -e<X<0 \text{ and } 0<Y<1 \tag{31}$$

For all of the four variables of U, V, θ, and θ_s, the basis function (ζ) is the same, and hence, the overall number of four nodes ($N = 4$) is required. Invoking the set of the basic functions introduced in Eqs. (30) and (31), the nonlinear residual equations (R_i^N) of the governing equations for momentum, Eqs. (28) and (29), together with the energy equations, Eqs. (17) and (18), can be derived as follows:

$$R_i^1=\sum_{k=1}^{N}\left(\frac{\rho_{hnf}}{\rho_{bf}}\right)U_k\int_\Omega\left[\left(\sum_{k=1}^{N}U_k\xi_k\right)\frac{\partial\xi_k}{\partial X}+\left(\sum_{k=1}^{N}V_k\xi_k\right)\frac{\partial\xi_k}{\partial Y}\right]\xi_i dXdY+\left(\sum_{k=1}^{N}U_k\int_\Omega\frac{\partial\xi_i}{\partial X}\frac{\partial\xi_k}{\partial X}dXdY+\sum_{k=1}^{N}V_k\int_\Omega\frac{\partial\xi_i}{\partial X}\frac{\partial\xi_k}{\partial Y}dXdY\right)+\frac{\mu_{hnf}}{\mu_{bf}}Pr\left[\sum_{k=1}^{N}U_k\int_\Omega\frac{\partial\xi_i}{\partial X}\frac{\partial\xi_k}{\partial X}dXdY+\sum_{k=1}^{N}U_k\int_\Omega\frac{\partial\xi_i}{\partial Y}\frac{\partial\xi_k}{\partial Y}dXdY\right] \tag{32}$$

$$R_i^2=\sum_{k=1}^{N}\left(\frac{\rho_{hnf}}{\rho_{bf}}\right)V_k\int_\Omega\left[\left(\sum_{k=1}^{N}U_k\xi_k\right)\frac{\partial\xi_k}{\partial X}+\left(\sum_{k=1}^{N}V_k\xi_k\right)\frac{\partial\xi_k}{\partial Y}\right]\xi_i dXdY+\left(\sum_{k=1}^{N}U_k\int_\Omega\frac{\partial\xi_i}{\partial Y}\frac{\partial\xi_k}{\partial X}dXdY+\sum_{k=1}^{N}V_k\int_\Omega\frac{\partial\xi_i}{\partial Y}\frac{\partial\xi_k}{\partial Y}dXdY\right)+\frac{\mu_{hnf}}{\mu_{bf}}Pr\left[\sum_{k=1}^{N}V_k\int_\Omega\frac{\partial\xi_i}{\partial X}\frac{\partial\xi_k}{\partial X}dXdY+\sum_{k=1}^{N}V_k\int_\Omega\frac{\partial\xi_i}{\partial Y}\frac{\partial\xi_k}{\partial Y}dXdY\right]+\frac{(\rho\beta)_{hnf}}{(\rho\beta)_{bf}}RaPr\left[\int_\Omega\left(\sum_{k=1}^{N}\theta_k\xi_k\right)\xi_i dXdY\right] \tag{33}$$

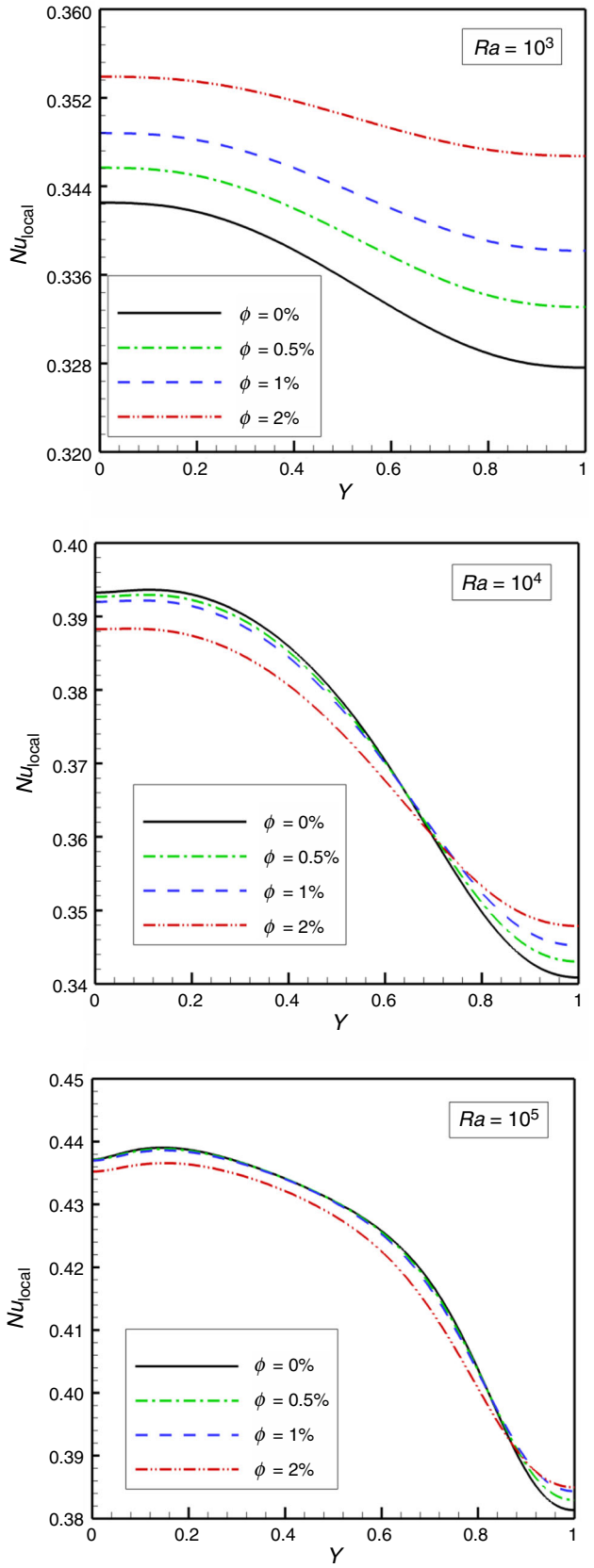

◀**Fig. 7** Evaluation of the local Nusselt number (Nu_{local}) on the hot side of the solid wall, for different values of the volume fraction of hybrid nanoparticles and $Ra = 10^3$, 10^4, and 10^5 when $R_k = 0.1$

$$R_i^3 = \sum_{k=1}^{N}\left(\frac{(\rho c_p)_{hnf}}{(\rho c_p)_{hf}}\right)\theta_k \int_{\Omega}\left[\left(\sum_{k=1}^{N} U_k\xi_k\right)\frac{\partial\xi_k}{\partial X} + \left(\sum_{k=1}^{N} V_k\xi_k\right)\frac{\partial\xi_k}{\partial Y}\right]\xi_i dXdY + \frac{k_{hnf}}{k_{bf}}\left(\sum_{k=1}^{N}\theta_k\int_{\Omega}\frac{\partial\xi_i}{\partial X}\frac{\partial\xi_k}{\partial X}dXdY + \sum_{k=1}^{N}\theta_k\int_{\Omega}\frac{\partial\xi_i}{\partial Y}\frac{\partial\xi_k}{\partial Y}dXdY\right) \tag{34}$$

$$R_i^4 = \sum_{k=1}^{N}\left(\frac{k_s}{k_{bf}}\right)\theta s_k \int_{\Omega}\frac{\partial\xi_i}{\partial X}\frac{\partial\xi_k}{\partial X}dXdY + \sum_{k=1}^{N}\left(\frac{k_s}{k_{bf}}\right)\theta s_k \int_{\Omega}\frac{\partial\xi_i}{\partial Y}\frac{\partial\xi_k}{\partial Y}dXdY \tag{35}$$

Solution procedure, grid independence tests, and validations

A non-uniform mesh, in which the mesh points are clustered near the walls, is utilized. The high-density mesh can capture the high boundary layer gradients next to the walls. The element ratio of 10 is utilized for the clustering of the mesh elements. The density of mesh points in the *x*-direction of the solid area is half of the cavity meshes. The density of mesh points in the *y*-direction of the solid area follows the patterns of the mesh points in the cavity. A schematic view of a coarse mesh with a size of 20 × 20 is depicted in Fig. 2. The number of the mesh points in the *x*-direction of the solid area is 10. This very low-density mesh is utilized to represent the selected grid. Much higher grid densities (i.e., 100 × 100 and more) were utilized for executing the grid independence tests. The results of the grid size examinations are presented in Table 2 when $Pr = 6.2$ and $R_k = 10$. Several grid sizes have been considered to assess grid independence. The corresponding average Nusselt numbers are compared. Comparing the results for both 0% and 1% of the hybrid nanoparticle, volume fraction confirms the fact that the optimal grid size is that of 100 × 100 elements.

Further validation has been done comparing the average Nusselt number with the work of Kahveci [45] by using the grid size of 100 × 100. Figure 3 shows the values of the Nusselt number versus the nanoparticle volume fraction for three values of the Rayleigh number. This figure confirms that the results of the present study are in good agreement with those reported by Kahveci [45] for all three cases of the Rayleigh numbers.

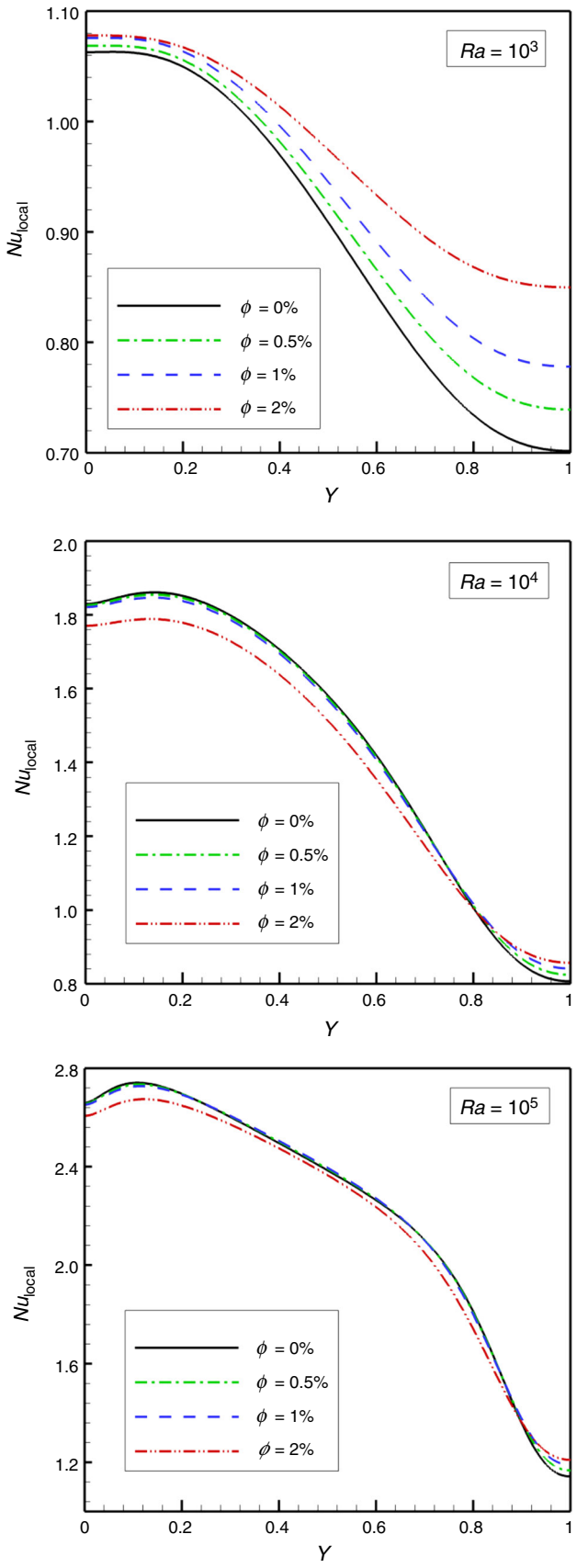

◀**Fig. 8** Evaluation of the local Nusselt number (Nu_{local}) on the hot side of the solid wall, for different values of the volume fraction of hybrid nanoparticles for $Ra = 10^3$, 10^4, and 10^5 in the case of $R_k = 1$

Results and discussion

To examine the effect of hybrid nanofluids upon natural convection flow and heat transfer, a square cavity with a side size of H and filled with Ag–MgO/water hybrid nanofluid has been envisioned. The results of the present analysis have been obtained with Rayleigh numbers in the interval of 10^3 and 10^5, and a nanoparticle volume fraction with a value between 0.0 and 0.02. The Prandtl number is fixed as $Pr = 6.2$.

Figures 4–6 show the dimensionless temperature contours of the Ag–MgO/water hybrid nanofluid for various volume fractions of the hybrid nanoparticles, Rayleigh number, and R_k. Figure 4 reveals that the temperature distribution in the cavity part is mostly a function of X for low values of the Rayleigh number. Further increases in the Rayleigh number from 10^3 to 10^5 indicate that the temperature distribution is significantly affected by Ra through the Y-axis, and becomes a function of both X and Y for large Rayleigh numbers. However, for a large R_k value (Fig. 6), it can be seen that the temperature distribution is a function of both X and Y even at low values of the Rayleigh number.

Interestingly, increasing the hybrid nanoparticle volume fraction changes the thickness of the thermal boundary layer. The change in the thickness of the thermal boundary layer is much more significant for low values of the Rayleigh number. For instance, for $Ra = 10^3$ and $R_k = 0.1$, the thickness of the thermal boundary layer significantly decreases as the volume fraction of the hybrid nanoparticles raises. Important to note is that the temperature distribution is profoundly affected by R_k, which represents the ratio between the thermal conductivity of the solid wall and that of the hybrid nanofluid. Comparison of the results of Figs. 4–6 indicates that as the value of R_k increases from 0.1 to 10, the thickness of the thermal boundary layer substantially augments.

Furthermore, the temperature distribution through the solid wall shows that as the value of R_k increases, the temperature difference throughout the conjugate wall considerably decreases. For example, the dimensionless temperature at both sides of the conjugate wall is approximately equal when the value of R_k is 10. When R_k is low, the thermal resistance of the solid wall is the dominant parameter of the heat transfer. Hence, the temperature distribution in the wall is almost linear. In this case, due to the low thermal conductivity of the solid wall, the heat transfer in the vertical direction is almost negligible.

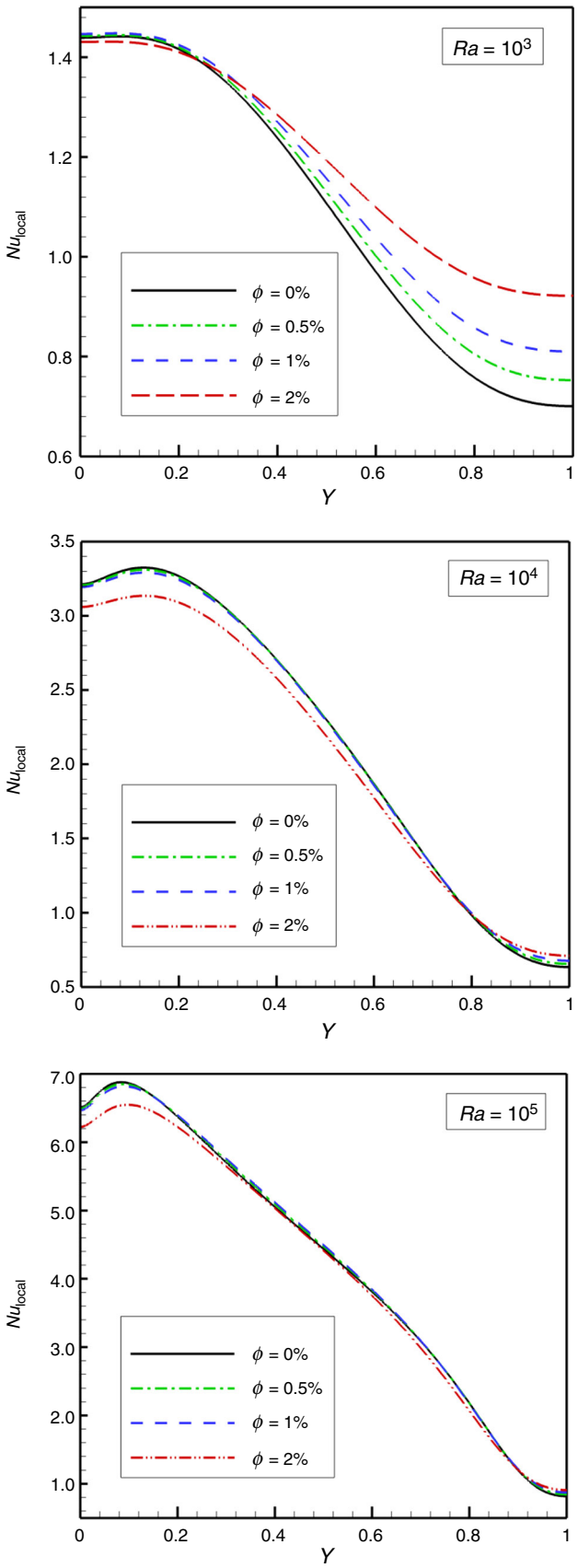

◀**Fig. 9** Evaluation of the local Nusselt number (Nu_{local}) on the hot side of the solid wall, for different values of the volume fraction of hybrid nanoparticles for $Ra = 10^3$, 10^4, and 10^5 in the case of $R_k = 10$

However, as the thermal conductivity of the solid wall increases, the temperature distribution inside the solid wall starts to show some nonlinear behaviors. In the case of $R_k = 1.0$, the nonlinear temperature gradients are more evident at the top of the solid wall where the flow starts to move along the horizontal wall of the cavity. At this region, the fluid velocity at the Y-direction (V) becomes strong, and hence, it commences to affect the temperature distribution in the solid wall in a normal direction. It should be noted that when $R_k = 1.0$, the conduction heat transfer in the solid wall is not strong enough to redistribute the temperature gradients.

When R_k is very high, the temperature gradient in the wall is very weak, and the solid wall is under significant influence from the hot wall boundary conditions. In this situation, the solid wall is almost at the temperature of the hot wall. However, as the Rayleigh number increases, the convective heat transfer gets stronger. As a result, when the Rayleigh number is high, i.e., $Ra = 10^5$, some temperature gradients can be observed at the bottom of the solid. This is where the convective heat transfer is high.

A comparison of the trends of the temperature contours in Figs. 4–6 reveals that when R_k is low, many of the temperature levels are inside the solid wall. This pattern indicates that most of the changes in the temperature gradient occur inside the solid wall. There are only a few temperature levels inside the fluid region, indicating small temperature gradients. Assuming a constant temperature level, the observed difference between the corresponding temperature levels of different volume fractions of nanoparticles becomes obvious. Indeed, as the solid wall acts as a thermal resistance (when R_k is low), the natural convective flow weakens, and the thermal diffusion mechanism grows in importance. Increasing the volume fraction of the nanoparticles produces a higher thermal conductivity in the nanofluid. Hence, as seen in Fig. 4 (the case of $Ra = 10^3$), the difference between the contours of the temperature distribution for various volume fractions of nanoparticles is accentuated. This is the case, in which the natural convective heat transfer is weakest. Generally, the increase in volume fraction of nanoparticles shifts the isotherms toward the hot wall at the top regions of the cavity. This is because of the increase in the viscosity of hybrid nanofluid by the increase in the volume fractions of nanoparticles.

Figures 7–9 present the variation of the local Nusselt number (Nu_{local}) on the hot side of the conjugate wall, at $X = 0$, for different values of the Rayleigh number, volume

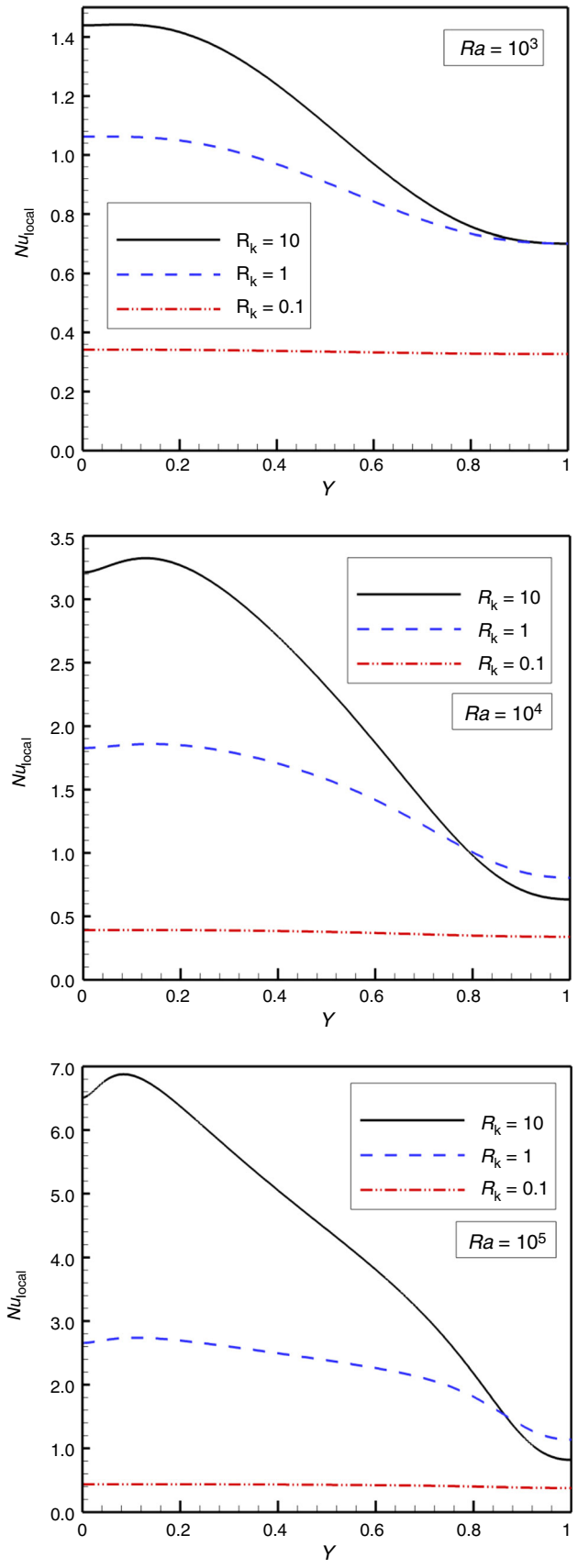

◀**Fig. 10** Evaluation of Local Nusselt number (Nu_{local}) on the hot side of the conjugate wall, for different values of the thermal conductivity ratio (R_k) for $Ra = 10^3$, 10^4, and 10^5, in the case of $\phi = 0\%$

fraction of the hybrid nanoparticles, and R_k. It can be seen that in all cases, the local Nusselt number is a decreasing function of Y. However, in some cases, there is a small augmentation at the bottom of the conjugate wall. The local Nusselt number is significantly affected by both the Rayleigh number and R_k. For instance, as R_k increases from 0.1 to 10, the values of the local Nusselt number at the bottom of the wall change from approximately 0.4–6.5 when $Ra = 10^5$. At the same location, when R_k is equal to 10, the value of the local Nusselt number increases from approximately 1.4–6.5, as the Ra increases from 10^3 to 10^5.

For low values of the Rayleigh number ($Ra = 10^3$), the local Nusselt number augments as the volume fraction of the hybrid nanoparticles increases from 0 to 0.02. The range of this change in the local Nusselt number is quite extensive at the upper half part of the cavity. Besides, for Ra equal to 10^3, it is evident that the enhancement in the local Nusselt number caused by the volume fraction of the hybrid nanoparticles is more significant for large values of R_k. In contrast, for large values of the Rayleigh number, the rise of the volume fraction of the nanoparticles reduces the local Nusselt number in a large portion of Y. It can also be seen that the effects of the hybrid nanoparticles on the local Nusselt number decline as the Rayleigh number augments.

The presence of nanoparticles in a nanofluid seems to enhance the thermal conductivity as well as the dynamic viscosity of the synthesized nanofluid. Increasing the thermal conductivity can enhance the thermal diffusivity and, consequently, boost heat transfer (Nusselt number). It is worth noting that an increase in the dynamic viscosity may reduce the fluid velocity and consequently the convective heat transfer. Indeed, when the convective heat transfer is low, the thermal diffusive mechanism is the dominant mechanism of heat transfer. Under these conditions, enhancement of heat transfer through an increase in the nanoparticle volume fraction can be expected (e.g., $Ra = 10^3$). The increase in Rayleigh number enhances the convective heat transfer mechanism (e.g., $Ra = 10^4$ and 10^5). Thus, a change in the trend of the Nusselt number as a function of the volume fraction of nanoparticles can be expected by the boost of the convective heat transfer mechanism.

Figure 10 illustrates the effects of the Rayleigh number and R_k on the local Nusselt number when the volume fraction of the hybrid nanoparticles is equal to 0. For $R_k = 0.1$, the local Nusselt number is approximately constant throughout the Y-direction and for any value of the Rayleigh number. As R_k increases, the local Nusselt number

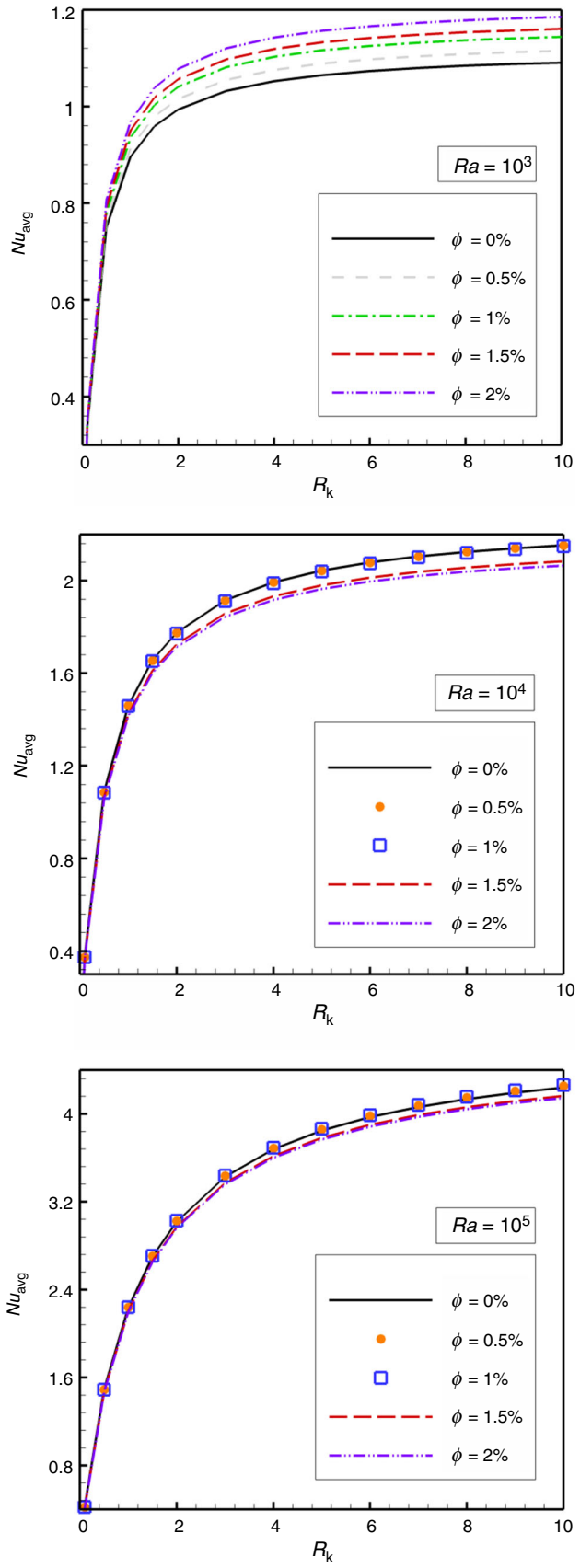

◀**Fig. 11** Average Nusselt number (Nu_{avg}) as a function of thermal conductivity ratio for various values of the volume fraction of hybrid nanoparticles for the cases of $Ra = 10^3$, 10^4, and 10^5

variation in the Y-direction becomes more substantial. For instance, when the Rayleigh number is equal to 10^5, the variation of the local Nusselt number in the Y-direction is approximately 0 in the case of $R_k = 0.1$, and then increases to approximately 6, when R_k is equal to 10. In the case of $R_k = 0.1$, the local Nusselt number is almost a horizontal line. This is since for low values of R_k the thermal resistance in the conjugate wall is dominant and the heat transfer is controlled by conduction in the wall.

The effects of the volume fraction of the hybrid nanoparticles, the Rayleigh number, and R_k on the values of the average Nusselt number are depicted in Fig. 11. The values of the average Nusselt number increase as the volume fraction of the hybrid nanoparticles increases, when $Ra = 10^3$. On the contrary, for larger Rayleigh numbers, the average Nusselt number declines as the volume fraction of the hybrid nanoparticles raise. Thus, according to Fig. 11, increasing the nanoparticle volume fraction could either increase or decrease the heat transfer rate: it depends entirely on the value of the Rayleigh number. Furthermore, the average Nusselt number is a growing function of R_k regardless of the magnitude of the Rayleigh number and of the volume fraction of the hybrid nanoparticles.

Conclusions

In the present study, the problem of conjugate natural convection inside a square cavity filled with an Ag–MgO/water hybrid nanofluid was investigated numerically. The finite element method was employed to numerically solve the governing partial differential equations representing the natural convection behavior of nanofluids. The effect of grid quality on the accuracy of the results was checked, and a non-uniform mesh with the size of 100×100 was selected. The effects of the dimensionless parameters, such as the Rayleigh number, the hybrid nanoparticle volume fraction, and R_k, upon the temperature distribution, local Nusselt number, and the average Nusselt number, are studied. The important observations of the present works are:

- Addition of the hybrid nanoparticles to the base fluid does not always enhance the heat transfer rate in the square cavity, which means that other parameters, such as the Rayleigh number, can change the effects of the hybrid nanoparticles.

- The local and average Nusselt numbers increase with increasing values of the volume fraction of hybrid nanoparticles for a small Rayleigh number. In contrast, increasing the volume fraction of the hybrid nanoparticles for large Rayleigh numbers reduces the values of the local and average Nusselt numbers.
- The temperature distribution and the thermal boundary layer thickness are profoundly affected by R_k, which represents the ratio between the solid wall thermal conductivity and that of the hybrid nanofluid.
- For large values of R_k, the local Nusselt number is statistically more significant at the bottom of the cavity. Moreover, the variation of the local Nusselt number throughout the Y-direction augments as the Rayleigh number increases.
- The average Nusselt number is an increasing function of both the Rayleigh number and R_k.

The results of the present study showed that using hybrid nanofluids does not always enhance the natural convection heat transfer in the cavity. Therefore, a comprehensive analysis of the effect of various types of hybrid nanofluids on the convective heat transfer in enclosures can be subject of future works.

References

1. Choi SU, Eastman JA. Enhancing thermal conductivity of fluids with nanoparticles. Lemont: Argonne National Lab; 1995.
2. Mahian O, Kolsi L, Amani M, Estellé P, Ahmadi G, Kleinstreuer C et al. Recent advances in modeling and simulation of nanofluid flows-part I: fundamental and theory. Phys Rep. 2019;790:1–48.
3. Mahian O, Kolsi L, Amani M, Estellé P, Ahmadi G, Kleinstreuer C et al. Recent advances in modeling and simulation of nanofluid flows-part II: applications. Phys Rep. 2019;791:1–59.
4. Alsabery A, Chamkha A, Saleh H, Hashim I. Heatline visualization of conjugate natural convection in a square cavity filled with nanofluid with sinusoidal temperature variations on both horizontal walls. Int J Heat Mass Transf. 2016;100:835–50.
5. Chamkha AJ, Jena SK, Mahapatra SK. MHD convection of nanofluids: a review. J Nanofluids. 2015;4(3):271–92.
6. Ismael MA, Armaghani T, Chamkha AJ. Conjugate heat transfer and entropy generation in a cavity filled with a nanofluid-saturated porous media and heated by a triangular solid. J Taiwan Inst Chem Eng. 2016;59:138–51.
7. Alsabery A, Sheremet M, Chamkha A, Hashim I. MHD convective heat transfer in a discretely heated square cavity with conductive inner block using two-phase nanofluid model. Sci Rep. 2018;8(1):7410.
8. Alnajem MHS, Alsabery AI, Hashim I, editors. Entropy generation and natural convection in a wavy-wall cavity filled with a nanofluid and containing an inner solid cylinder. IOP Conference Series: Materials Science and Engineering. Bristol: IOP Publishing; 2019.
9. Alsabery AI, Gedik E, Chamkha AJ, Hashim I. Effects of two-phase nanofluid model and localized heat source/sink on natural convection in a square cavity with a solid circular cylinder. Comput Methods Appl Mech Eng. 2019;346:952–81.
10. Alsabery A, Ismael M, Chamkha A, Hashim I. Effects of two-phase nanofluid model on MHD mixed convection in a lid-driven cavity in the presence of conductive inner block and corner heater. J Therm Anal Calorim. 2019;135(1):729–50.
11. Sheremet MA, Pop I. Marangoni natural convection in a cubical cavity filled with a nanofluid. J Therm Anal Calorim. 2019;135(1):357–69.
12. Sheikholeslami M, Sheremet MA, Shafee A, Li Z. CVFEM approach for EHD flow of nanofluid through porous medium within a wavy chamber under the impacts of radiation and moving walls. J Therm Anal Calorim. 2019. https://doi.org/10.1007/s10973-019-08235-3.
13. Revnic C, Ghalambaz M, Groşan T, Sheremet M, Pop I. Impacts of non-uniform border temperature variations on time-dependent nanofluid free convection within a trapezium: Buongiorno's nanofluid model. Energies. 2019;12(8):1461.
14. Kameya Y, Hanamura K. Enhancement of solar radiation absorption using nanoparticle suspension. Sol Energy. 2011;85(2):299–307.
15. Chen M, He Y, Zhu J, Shuai Y, Jiang B, Huang Y. An experimental investigation on sunlight absorption characteristics of silver nanofluids. Sol Energy. 2015;115:85–94.
16. Padmavathy N, Vijayaraghavan R. Enhanced bioactivity of ZnO nanoparticles—an antimicrobial study. Sci Technol Adv Mater. 2008;9(3):035004.
17. Bindhu M, Umadevi M. Antibacterial and catalytic activities of green synthesized silver nanoparticles. Spectrochim Acta Part A Mol Biomol Spectrosc. 2015;135:373–8.
18. Xuan Y, Duan H, Li Q. Enhancement of solar energy absorption using a plasmonic nanofluid based on TiO_2/Ag composite nanoparticles. RSC Adv. 2014;4(31):16206–13.
19. Madhesh D, Parameshwaran R, Kalaiselvam S. Experimental investigation on convective heat transfer and rheological characteristics of Cu–TiO_2 hybrid nanofluids. Exp Thermal Fluid Sci. 2014;52:104–15.
20. Sundar LS, Singh MK, Sousa AC. Enhanced heat transfer and friction factor of MWCNT–Fe_3O_4/water hybrid nanofluids. Int Commun Heat Mass Transf. 2014;52:73–83.
21. Sarkar J, Ghosh P, Adil A. A review on hybrid nanofluids: recent research, development and applications. Renew Sustain Energy Rev. 2015;43:164–77.
22. Esfe MH, Arani AAA, Rezaie M, Yan W-M, Karimipour A. Experimental determination of thermal conductivity and dynamic viscosity of Ag–MgO/water hybrid nanofluid. Int Commun Heat Mass Transf. 2015;66:189–95.
23. Esfe MH, Saedodin S, Biglari M, Rostamian H. Experimental investigation of thermal conductivity of CNTs–Al_2O_3/water: a statistical approach. Int Commun Heat Mass Transf. 2015;69:29–33.
24. Esfe MH, Yan W-M, Akbari M, Karimipour A, Hassani M. Experimental study on thermal conductivity of DWCNT–ZnO/water-EG nanofluids. Int Commun Heat Mass Transf. 2015;68:248–51.
25. Huang D, Wu Z, Sunden B. Effects of hybrid nanofluid mixture in plate heat exchangers. Exp Thermal Fluid Sci. 2016;72:190–6.
26. Nimmagadda R, Venkatasubbaiah K. Conjugate heat transfer analysis of micro-channel using novel hybrid nanofluids. Eur J Mech B Fluids. 2015;52:19–27.
27. Ghalambaz M, Doostani A, Chamkha AJ, Ismael MA. Melting of nanoparticles-enhanced phase-change materials in an enclosure: effect of hybrid nanoparticles. Int J Mech Sci. 2017;134:85–97.
28. Chamkha A, Doostanidezfuli A, Izadpanahi E, Ghalambaz MJAPT. Phase-change heat transfer of single/hybrid nanoparticles-enhanced phase-change materials over a heated horizontal

cylinder confined in a square cavity. Adv Powder Technol. 2017;28(2):385–97.
29. Mehryan S, Kashkooli FM, Ghalambaz M, Chamkha AJJAPT. Free convection of hybrid Al_2O_3–Cu water nanofluid in a differentially heated porous cavity. Adv Powder Technol. 2017;28(9):2295–305.
30. Ben-Nakhi A, Chamkha AJ. Conjugate natural convection in a square enclosure with inclined thin fin of arbitrary length. Int J Therm Sci. 2007;46(5):467–78.
31. Ben-Nakhi A, Chamkha AJ. Conjugate natural convection around a finned pipe in a square enclosure with internal heat generation. Int J Heat Mass Transf. 2007;50(11):2260–71.
32. Shenoy A, Sheremet M, Pop I. Convective flow and heat transfer from wavy surfaces: viscous fluids, porous media, and nanofluids. Boca Raton: CRC Press; 2016.
33. Sheremet MA, Pop I, Bachok N. Effect of thermal dispersion on transient natural convection in a wavy-walled porous cavity filled with a nanofluid: Tiwari and Das' nanofluid model. Int J Heat Mass Transf. 2016;92:1053–60.
34. Sheremet MA, Miroshnichenko IV. Numerical study of turbulent natural convection in a cube having finite thickness heat-conducting walls. Heat Mass Transf. 2015;51(11):1559–69.
35. Chamkha AJ, Ismael MA. Conjugate heat transfer in a porous cavity heated by a triangular thick wall. Numer Heat Transf Part A Appl. 2013;63(2):144–58.
36. Chamkha AJ, Ismael MA. Conjugate heat transfer in a porous cavity filled with nanofluids and heated by a triangular thick wall. Int J Therm Sci. 2013;67:135–51.
37. Kuznetsov GV, Sheremet M. Unsteady natural convection of nanofluids in an enclosure having finite thickness walls. Comput Therm Sci Int J. 2011; 3(5):427–43.
38. Sheremet MA, Pop I, Shenoy A. Unsteady free convection in a porous open wavy cavity filled with a nanofluid using Buongiorno's mathematical model. Int Commun Heat Mass Transf. 2015;67:66–72.
39. Sheremet MA, Pop I. Conjugate natural convection in a square porous cavity filled by a nanofluid using Buongiorno's mathematical model. Int J Heat Mass Transf. 2014;79:137–45.
40. Soltani O, Akbari M. Effects of temperature and particles concentration on the dynamic viscosity of MgO-MWCNT/ethylene glycol hybrid nanofluid: experimental study. Physica E. 2016;84:564–70.
41. Kefayati GR. Effect of a magnetic field on natural convection in an open cavity subjugated to water/alumina nanofluid using lattice Boltzmann method. Int Commun Heat Mass Transf. 2013;40:67–77.
42. Costa V. Natural convection in partially divided square enclosures: effects of thermal boundary conditions and thermal conductivity of the partitions. Int J Heat Mass Transf. 2012;55(25):7812–22.
43. Nasrin R, Alim M. Free convective flow of nanofluid having two nanoparticles inside a complicated cavity. Int J Heat Mass Transf. 2013;63:191–8.
44. Reddy JN. An introduction to the finite element method, vol. 2.2. New York: McGraw-Hill; 1993.
45. Kahveci K. Buoyancy driven heat transfer of nanofluids in a tilted enclosure. J Heat Transf. 2010;132(6):062501.